Chaotic dynamics of a piecewise cubic map

Firdaus E. Udwadia and Ramesh S. Guttalu
Department of Mechanical Engineering, University of Southern California, Los Angeles, California 90089-1453
(Received 2 February 1989)

An analytical study of the dynamics of a piecewise cubic map depending on two parameters is carried out in this paper. For this type of map, it is shown that a stable fixed point coexists with a chaotic attractor. The way in which the deterministic dynamics of the map undergoes chaos is not representable by means of the standardly proposed routes to chaos. It appears that in this case the chaos is initiated by the appearance of an unstable solution born out of a tangent bifurcation. The general geometric approach presented here in obtaining the analytical results does not make use of the Schwarzian curvature of the map. Moreover, it is shown that only the first few iterates essentially describe the global dynamics of the map. The methodology presented here could be used to good advantage for understanding the dynamics of other types of maps as well. Computational results are provided by the cell-mapping method to expose and confirm the analytical results given in this paper.

I. INTRODUCTION

The study of iterated maps is becoming an important aspect of the study of nonlinear systems; see Bernussou,[1] Collet and Eckmann,[2] and Devaney.[3] Such maps have been of interest to population biologists, mathematicians, engineers, physicists, and chemists to name but a few disciplines in which their application arises; see Berge *et al.*,[4] Guckenheimer and Holmes, [5] Lichtenberg and Lieberman,[6] Moon,[7] Thompson and Stewart,[8] and Zaslavsky.[9] Though great strides have been made in the last ten years or so in deciphering the nature of the iterated trajectories, there are several simple maps which often arise in practical applications which appear to fall beyond those for which general results are available today. This paper considers one such map which occurs commonly in mechanical and structural systems. It is described by the two-parameter family given by

$$x_{n+1}=f(x_n)=\begin{cases}\alpha x_n+\beta x_n^3, & 0\le x_n\le \frac{1}{2}\\ \alpha(1-x_n)+\beta(1-x_n)^3, & \frac{1}{2}\le x_n\le 1.\end{cases} \tag{1}$$

Here, β is restricted to the range $[0,4(2-\alpha)]$ so that $f:[0,1]\to[0,1]$, and α is restricted to be non-negative.

Several studies have been conducted on one-dimensional cubic maps. We only cite a few references here: Chavoya-Aceves and Angulus-Brown,[10] Arecchi *et al.*,[11] Testa and Held,[12] Hu and Mao,[13] Pikovsky,[14] Fraser and Kapral,[15] Rogers and Whitley,[16] and Holmes.[17] The map given by (1) differs from the maps analyzed in the above references in that it is a piecewise continuous function and it depends on two parameters. Moreover, we undertake a geometrical approach to understand the dynamics of the map and substantiate this with computational results.

Maps of the form (1) often arise as point maps obtained from differential equations (for example, the van der Pol oscillator and Poincaré sections of the Lorenz map; see Berge *et al.*[4]). Yet the map is not C^1 and its Schwarzian curvature depends on the parameters α and β as shown below,

$$Sf(x)=\begin{cases}\dfrac{6\beta(\alpha-6\beta x^2)}{(\alpha+3\beta x^2)^2}, & 0\le x_n\le \frac{1}{2}\\ \dfrac{6\beta(\alpha-6\beta(1-x)^2)}{[\alpha+3\beta(1-x)^2]^2}, & \frac{1}{2}\le x_n\le 1.\end{cases} \tag{2}$$

The Schwarzian curvature is positive for $x<(\alpha/6\beta)^{1/2}$ and $x>1-(\alpha/6\beta)^{1/2}$. For example, the Schwarzian curvature is positive for $x\in[0,1]$ when $\beta<\frac{2}{3}\alpha$.

The techniques that we use appear to be generic in nature, especially for symmetric maps. They rely crucially on the geometrical interpretation of the successive maps. It is shown that the first few iterates of the peak of the map are sufficient in unravelling the global dynamic behavior of the system. The advantage of the approach is that analyses similar to the one performed here can be applied to other maps which have both negative Schwarzian curvature (like the logistic map) and positive curvature [like the map given by Eq. (1)].

The cubic map given by Eq. (1) displays a route to chaos which is nonstandard. The transition to chaos is born from a tangent bifurcation which immediately explodes through the development of an infinite number of unstable fixed points. Unlike the logistic map, the modulus of the slope of the cubic map given by (1) in an ϵ neighborhood around this tangent bifurcation point is always greater than unity. Hence, the unusual route to chaos. In addition, for certain ranges of parameters α and β, a stable fixed point coexists with the chaotic attractor. This chaotic attractor, in turn, for a certain range of parameter values, becomes a period two chaotic attractor with each trajectory alternatively visiting each of its two pieces.

In Sec. II, we begin with analytical results of the cubic map f followed by their computational verification and exposition. The Appendix briefly deals with the details of the computational technique of cell-to-cell mapping used in Sec. II. Concluding remarks appear in Sec. III.

II. PROPERTIES OF THE CUBIC MAP f

We present results regarding the dynamic behavior of the map f. Neither the shape of the map nor specific reference to its Schwarzian curvature is needed to arrive at the results presented in this section.

Lemma 1. If $\alpha<1$ ($\alpha>1$), the fixed point $x=0$ is an asymptotically stable (unstable) fixed point.

Proof. Noting that $f'(x)=\alpha+3\beta x^2$, $x\in[0,\frac{1}{2}]$, the result is obvious. ■

Lemma 2. If $\alpha<1$ and $\beta<4(1-\alpha)$, then the map f has only one asymptotically stable fixed point at $x=0$. The entire interval [0,1] is attracted towards this attracting fixed point.

Proof. In the region $I_L=[0,\frac{1}{2}]$, for a period one solution we require

$$\alpha x_1^* + \beta x_1^{*3} = x_1^*, \quad x_1^* \in I_L \tag{3}$$

so that

$$x_1^* = \left[\frac{1-\alpha}{\beta}\right]^{1/2} \tag{4}$$

which exists for $\beta \geq 4(1-\alpha)$. Note that $f'(x_1^*)=3-2\alpha>1$ for $\alpha<1$ and x_1^* is always unstable. Choosing $x_1^*=\frac{1}{2}$ and noting that under the stipulated conditions $f(x_1^*)<\frac{1}{2}$, the entire interval [0,1] is attracted to $x=0$. ■

Note that for $\beta<4(1-\alpha)$, $x_1^*\in I_L$ coalesces with $x=0$ and $x=0$ is the only fixed point which is stable. When $\beta=4(1-\alpha)$, except for the unstable fixed point $x_1^*=\frac{1}{2}$, the result of Lemma 2 is applicable.

Lemma 3. For $\alpha<1$ and $\beta>4(1-\alpha)$, the map f has three fixed points.

Proof. In addition to the stable fixed point at $x=0$, we have a fixed point at $x=x_1^*$, where x_1^* is given by (4) and at $x=x_2^*$, where

$$x_2^* = 1-y \tag{5}$$

and y is the real root of the cubic equation

$$\beta y^3+(1+\alpha)y-1=0 \ . \tag{6}$$

■

Equation (6) has only one real root given by

$$y = r^{1/3} - \frac{1+\alpha}{3\beta r^{1/3}} \ , \qquad r(\alpha,\beta)=\frac{1}{2\beta}\left[1+\left[1+\frac{4(1+\alpha)^3}{27\beta}\right]^{1/2}\right] \tag{7}$$

for $\beta>0$. When $\beta=0$, then $y=1/(1+\alpha)$, $x_2^*=\alpha/(1+\alpha)$. We note that the fixed point at $x=0$ has the interval $[0,x_1^*)$ and $(1-x_1^*,1]$ as its region of attraction. Both x_1^* and x_2^* are unstable fixed points throughout the range of interest of α and β.

Lemma 4. Consider the set of points

$$\{y_i\}=\{y\,|\,f^k(y)=\tfrac{1}{2} \text{ for some k}, \ 0\leq k<n\} \ . \tag{8}$$

These points y_i divide the interval [0,1] into subintervals, over each of which the iterate f^n is monotone.

Proof. Let x and x' be two points which are inside a subinterval. Their (symbolic) itineraries coincide for the indices $i\in(0,n-1)$; for if they did not then there exists a $j<n$, such that $f^j(x)<\frac{1}{2}$ and $f^j(x')>\frac{1}{2}$. Thus by continuity there must be a point y between x and x' for which $f^j(y)=\frac{1}{2}$, a contradiction with the statement of our set $\{y_i\}$. Since the itineraries coincide, f^n is a homeomorphism because f is a homeomorphism on any interval that does not contain $x=\frac{1}{2}$ within it. ■

In what follows, we shall show that the behavior of the trajectories of (1) critically depend on the first few iterates of the point $x=\frac{1}{2}$. We denote those points for convenience as follows:

$$\begin{aligned} &A=(\tfrac{1}{2},f_{\max}); \quad f_{\max}=f(\tfrac{1}{2})=\tfrac{1}{8}(4\alpha+\beta) \ , \\ &D=(f_{\max},f^2(\tfrac{1}{2})); \quad f(f_{\max})=f^2(\tfrac{1}{2}) \ , \\ &E=(f^2(\tfrac{1}{2}),f^3(\tfrac{1}{2})) \ , \\ &C=(f^3(\tfrac{1}{2}),f^4(\tfrac{1}{2})) \ , \\ &B=(f^4(\tfrac{1}{2}),f^5(\tfrac{1}{2})) \ , \\ &F=(f^5(\tfrac{1}{2}),f^6(\tfrac{1}{2})) \ . \end{aligned} \tag{9}$$

See Fig. 1 for an illustration for the sequence of the mapping: $A\to D\to E\to C\to B\to F$. Relative locations of these points depend on the values of α and β. We denote the x coordinates of these points by x_A,x_B,x_C,x_D,x_E,x_F and y coordinates by y_A,y_B,y_C,y_D,y_E,y_F, respectively. The two dashed lines in Fig. 1 are straight lines with slopes $+1$ and -1.

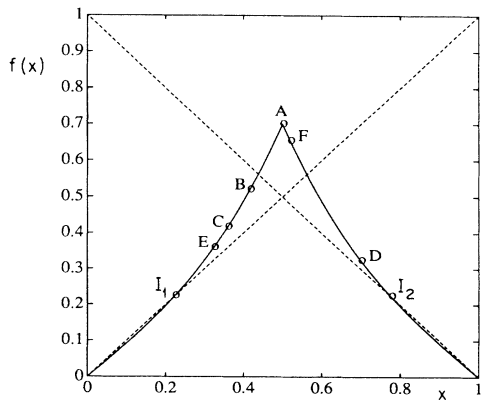

FIG. 1. Location of points of first five maps of $f(x)$ starting at $x=\frac{1}{2}$ for $\alpha=0.90$ and $\beta=2.0$. Also shown are the location of points I_1 and I_2.

Lemma 5. The requirement that $x_D = f_{\max} = 1 - x_1^*$ *is fulfilled when either* $\beta_c = 4(1-\alpha)$ *or* $\beta_d \equiv \phi(\alpha) = 2[3-\alpha-\sqrt{(1-\alpha)(5-\alpha)}]$.

Proof. For $f_{\max} = 1 - x_1^*$, we require

$$\beta^3 - 8(2-\alpha)\beta^2 + 16(2-\alpha)^2\beta - 64(1-\alpha) = 0 \ . \tag{10}$$

Noting that $\alpha \geq 0$, Eq. (10) is satisfied when

$$\beta_c = 4(1-\alpha) \tag{11}$$

or

$$\beta_d = 2[3-\alpha-\sqrt{(1-\alpha)(5-\alpha)}] \ . \tag{12}$$

■

The root $\beta_c = 4(1-\alpha)$ of (10) corresponds to the situation when the point A is a fixed point of the map f, causing the points A, B, C, D, and E to coincide. For $\alpha = \frac{1}{2}$, $\beta_c = \beta_d = 2$. For $\alpha = 1$, $\beta_c = 0$, $\beta_d = 4$. The root β_d of (10) is not meaningful in describing the trajectories of the system (1) for $\alpha < \frac{1}{2}$, for then $\beta_d < \beta_c = 4(1-\alpha)$ (in this case the only fixed point is at $x = 0$). This situation [that is, $\alpha < 1$ and $\beta \leq 4(1-\alpha)$] has been dealt with in Lemma 2. When $\beta > \beta_d$, $x_D > 1 - x_1^*$.

Lemma 6. For $\frac{1}{2} < \alpha < 1$ *and* $\beta_d < \beta \leq 4(2-\alpha)$, *the graph of* $f^n(x)$ *has* 2^{n-1} *maxima and* $2^{n-1}-1$ *minima in the interval* $(x_1^*, 1-x_1^*)$.

Proof. It is easy to show upon argument by contradiction that excluding the points $x = 0$ and $x = 1$, the maxima and minima lie between $(x_1^*, 1-x_1^*)$. This is because $x_1^* < \frac{1}{2}$ and the region between $(0, x_1^*)$ and $(1-x_1^*, 1)$ is attracted to the stable fixed point at $x = 0$.

Regarding the number of maxima and minima, this is true by inspection for f^2. Assume that this is true for f^n. Further assume that the range of variation of each adjacent pair of maxima and minima includes $x = \frac{1}{2}$ (this is true of the map f^2). Then at the next iteration, between each pair of adjacent maxima we will have two new maxima. Thus we will have $2(2^{n-1}-1)$ maxima. In addition, by similar argument we will have two maxima, one on either side of the left-most and right-most maxima of f^n. Thus, the total maxima of f^{n+1} will be $2(2^{n-1}-1) + 2 = 2^n$. Since $x_d > 1 - x_1^*$, each minimum remains to be a minimum. Therefore, the graph of f^{n+1} between any minimum and its immediately adjacent maximum must span $\frac{1}{2}$. The minima tend to zero as $n \to \infty$ because the fixed point at $x = 0$ is a stable attractor. ■

We note that since two new maxima of f^{n+1} appear between each pair of maxima of f^n, the spacing between maxima decreases. The situation depicted by Lemma 6 is shown in Figs. 2(a)–2(d). Plots of f, f^2, f^4, and f^9 are shown for $\alpha = 0.9$ and $\beta = 3.5$.

Lemma 7. For $\frac{1}{2} < \alpha < 1$ *and* $\beta_d < \beta \leq 4(2-\alpha)$, *given any point* $x \in (x_1^*, 1-x_1^*)$ *and an* $\epsilon > 0$, *there exists an* n *such that* $f^n(x)$ *is in an* ϵ *neighborhood of the point* A.

Proof. As n increases, the number of maxima of f^n between any two adjacent maxima increases. The result follows by Lemma 6. ■

We have thus shown that for any point $x \in (x_1^*, 1-x_1^*)$, the trajectory of (1) passes infinitesimally close to A.

Theorem 1. For $\frac{1}{2} < \alpha < 1$ *and* $\beta_d < \beta \leq 4(2-\alpha)$, *almost all trajectories are attracted to the asymptotically stable fixed point* $x = 0$.

Proof. Any trajectory of (1) that begins in the interval $[0, x_{I_1})$ or $(x_{I_2}, 1]$ is attracted to $x = 0$ by Lemma 1 (see Fig. 1). Trajectories that begin in the interval $x \in (x_1^*, 1-x_1^*)$ pass arbitrarily close to A (by Lemma 7) which then map to D. Since $x_D > 1 - x_1^*$ for the given range of α and β, D is attracted to $x = 0$. Hence the result follows. ■

We note that trajectories of (1) that begin at x_1^* and $1-x_1^*$ converge to the unstable fixed point $x = x_1^*$. We also note that the points I_1 and I_2 (Fig. 1) map to the unstable point I_1. Thus at $\beta = \beta_d$ (that is, $x_D = 1 - x_1^*$) the point $x = \frac{1}{2}$ maps to I_1 and the points B, C, and E coincide.

Theorem 2. For $\alpha \leq \frac{1}{2}$ *and* $4(1-\alpha) \leq \beta \leq 4(2-\alpha)$, *almost all trajectories are asymptotically attracted to the stable fixed point* $x = 0$.

Proof. When $\alpha = \frac{1}{2}$, $\beta_d = 2$. For $\alpha \leq \frac{1}{2}$, $\beta \geq \beta_d$ so that $x_D > 1 - x_1^*$ and the arguments of Lemma 6, Lemma 7, and Theorem 1 apply. ■

Lemma 8. For $\frac{1}{2} < \alpha < 1$ *and* $4(1-\alpha) < \beta < \beta_d$, *trajectories of the map* f *either (a) asymptotically map to the fixed point* $x = 0$ *or (b) remain trapped in the region* $[x_1^*, 1-x_1^*]$.

Proof. (a) Trajectories of (1) that lie in $[0, x_1^*)$ or $(1-x_1^*, 1]$ are attracted to the fixed point $x = 0$. (b) We note that since $\beta < \beta_d$, $x_D < 1 - x_1^*$ and $x_E > x_1^*$. For any point $x \in (x_1^*, 1-x_1^*)$, $f(x) \in (x_1^*, 1-x_1^*)$ and the same holds for any iterate $f^n(x)$. Hence the result. If x is one of the end points of the interval, the result is obvious. ■

Lemma 9. For $\frac{1}{2} < \alpha < 1$ *and* $4(1-\alpha) < \beta < \beta_d$, *all trajectories of (1) which start in* $[x_E, x_D]$ *remain in that interval for all* n.

Proof. Noting that A maps to D and D maps to E, the proof is identical to Lemma 8. ■

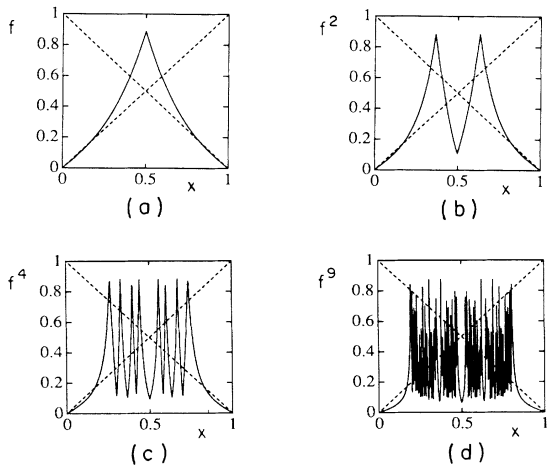

FIG. 2. (a)–(d) f, f^2, f^4, and f^9 maps for $\alpha = 0.9$ and $\beta = 3.5$ showing the increasing number of maxima of f^n.

Lemma 10. For $\frac{1}{2}<\alpha<1$ *and* $4(1-\alpha)<\beta<\beta_d$, *trajectories of (1) that begin in the interval* $(x_1^*, x_E]$ *or in* $[x_D, 1-x_1^*)$ *eventually get trapped in the interval* $[x_E, x_D]$.

Proof. Notice that $|f'(x)|>1$ for x belonging to either of the two intervals. Hence, at each iteration of x we obtain gradually increasing values of the iterates until the iterate becomes larger than x_E and by Lemma 9 the result follows. We note that no iterate can exceed x_D. ■

Theorem 3. For $\frac{1}{2}<\alpha<1$ *and* $4(1-\alpha)<\beta<\beta_d$, *trajectories of (1) that start in* $(x_1^*, 1-x_1^*)$ *are asymptotically trapped in the interval* $[x_E, x_D]$ *and the regions* $(x_1^*, x_E]$ *and* $[x_D, 1-x_1^*)$ *are attracted to this interval.* ■

Proof. Using Lemmas 9 and 10 the result follows.

Figure 3(a) shows the map f for $\alpha=0.75$ and $\beta=2.2$ together with the locations of the first few iterates of the point $x=\frac{1}{2}$. Here, $x_A=\frac{1}{2}$, $x_D=0.65$, $x_E=0.356\,825$, $x_C=0.367\,570\,063\,2$, $x_B=0.384\,932\,989\,7$, and $x_F=0.414\,180\,773\,5$. Also, $x_1^*=0.337\,099\,931\,2$. Numerically computed f^{5000} is shown in Fig. 3(b) for the same parameter values. The figure shows the trapped trajectory between x_E and x_D. The stable point at $x=0$ attracts the intervals $[0, x_1^*)$ and $(1-x_1^*, 1]$.

Theorem 4. For $\frac{1}{2}<\alpha<1$ *and* $4(1-\alpha)<\beta<\beta_d$, *the fixed points of* f^n *are all unstable for* $x\in[x_1^*, 1-x_1^*]$.

Proof. Noting the chain rule for the derivative for f^n and that $|f'(x)|>1$ for $x\in[x_1^*, 1-x_1^*]$, the result is obtained by using Theorem 3. ■

Figure 4(a) shows the variation in x_D, x_E, x_1^*, and x_2^*

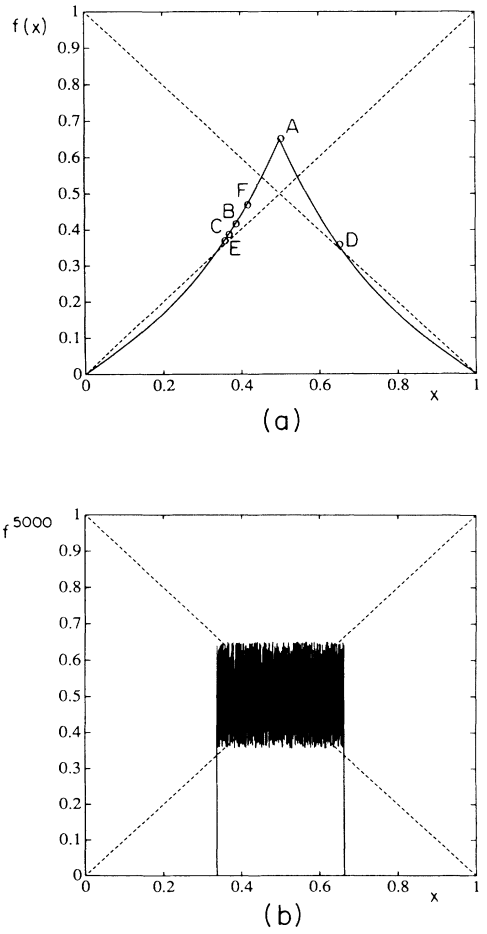

FIG. 3. (a) Map f for $\alpha=0.75$ and $\beta=2.2$. (b) f^{5000} map for $\alpha=0.75$ and $\beta=2.2$ showing the trapped trajectory.

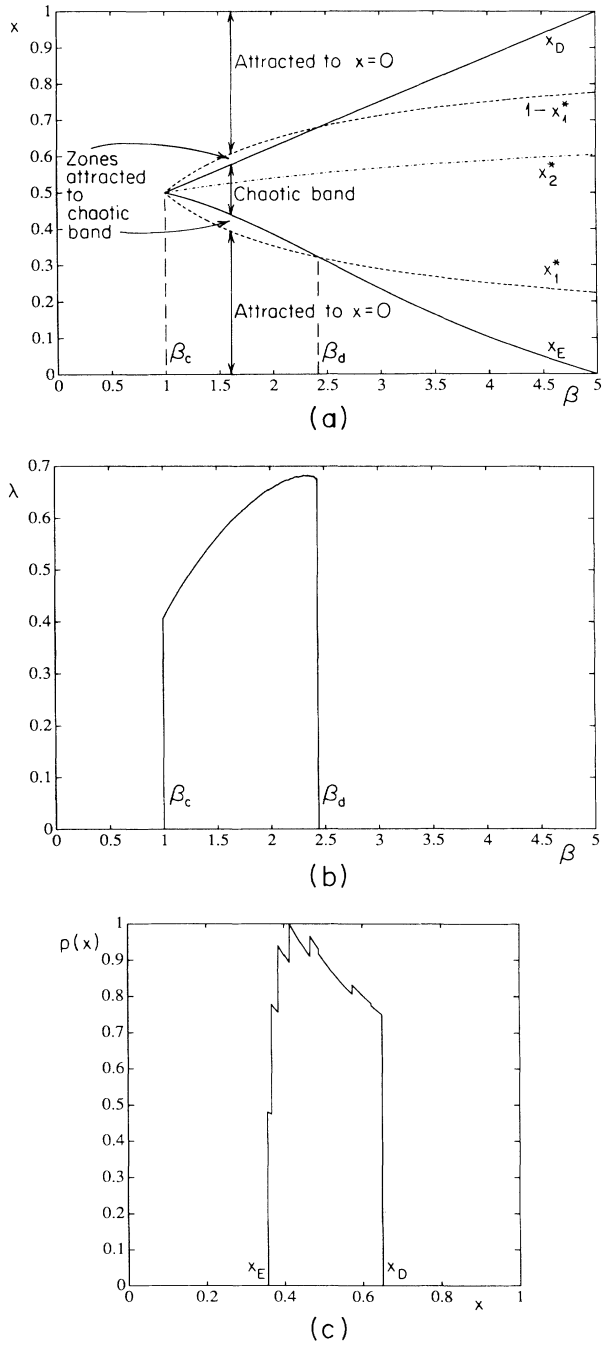

FIG. 4. (a) Chaotic band as a function of β for the map f for $\alpha=0.75$. (b) Liapunov exponent of the chaotic band for $\alpha=0.75$ as a function of β. (c) Long-term probability distribution of the states in the chaotic region for $\alpha=0.75$ and $\beta=2.2$.

as a function of β for $\alpha=0.75$. This figure indicates the chaotic band between x_E and x_D for the map of Fig. 3. Figure 4(b) displays the numerically computed Liapunov exponent for the chaotic band showing the sensitive dependence to initial conditions for values of $\beta<\beta_d$. The Liapunov exponent λ for the map f was calculated using the definition

$$\lambda=\lim_{N\to\infty}\frac{1}{N}\sum_{n=1}^{N}\ln|f'(x_n)|\ .$$

We note that for $\alpha=0.75$, $\beta_c=1.0$ and $\beta_d=2.438\,447\,18$. As another check, the long-term probability distribution of states in the chaotic band is computed for $\beta=2.2$ and is shown in Fig. 4(c). The invariant probability distribution was computed following a procedure described in Lichtenberg and Lieberman.[6] The chaotic attractor is contained in the interval $[x_E,x_D]$ and attracts the integral $[x_1^*,1-x_1^*]$ as expected by Theorem 3.

Lemma 11. For $\alpha>1$ and $0<\beta<4(2-\alpha)$, the map f has two fixed points which are both unstable.

Proof. The fixed points are at $x=0$ and $x=x_2^*$ given by Eqs. (5) and (6). These are both clearly unstable. ■

We note that as $\alpha\to1^-$ (that is, α approaches 1 from below), $x_1^*\to0$, making $x=0$ an unstable fixed point. Also $x_D>\frac{1}{2}$.

Theorem 5. For $\alpha>1$ and $0<\beta<4(2-\alpha)$, all the trajectories of (1) that begin in (0,1) are asymptotically trapped in the interval $[x_E,x_D]$.

Proof. The proof follows by arguments similar to those of Lemmas 8–11 and Theorem 3, by setting $x_1^*=0$. ■

Theorem 6. For $\alpha>1$ and $0<\beta<4(2-\alpha)$, the fixed points of f^n are all unstable. ■

Proof. The proof is similar to Theorem 4, noting that $x_1^*=0$.

The types of solutions that these analytical results provide over the domain of interest in α and β, namely, for $\alpha\in[0,2]$ and $\beta\in[0,4(2-\alpha)]$, are illustrated in Fig. 5, where the region of concern is the lower triangular region. We summarize our results regarding the dynamics of the map f as follows.

(1) For $0<\alpha<\frac{1}{2}$ and $0<\beta<4(2-\alpha)$, almost all trajectories of (1) are attracted to the asymptotically stable fixed point $x=0$.

(2) For $\frac{1}{2}<\alpha<1$ and $0<\beta<4(1-\alpha)$, all trajectories of (1) are attracted to the asymptotically stable fixed point $x=0$.

(3) For $\frac{1}{2}<\alpha<1$ and $(1-\alpha)<\beta<\beta_d$, all trajectories of (1) that start in $(x_1^*,1-x_1^*)$ are attracted to the interval $[x_E,x_D]$; trajectories that start in the intervals $[0,x_1^*)$ and $(1-x_1^*,1]$ are attracted to the asymptotically stable fixed point at $x=0$. The trajectories which are trapped in $[x_E,x_D]$ are chaotic.

(4) For $\frac{1}{2}<\alpha<1$ and $\beta_d<\beta\le4(2-\alpha)$, almost all trajectories of (1) will be attracted to the asymptotically stable fixed point $x=0$.

(5) For $1<\alpha\le2$ and $0<\beta<4(2-\alpha)$, all trajectories of (1) which start in (0,1) will be attracted to the interval $[x_E,x_D]$. All trajectories within this attractor will be chaotic.

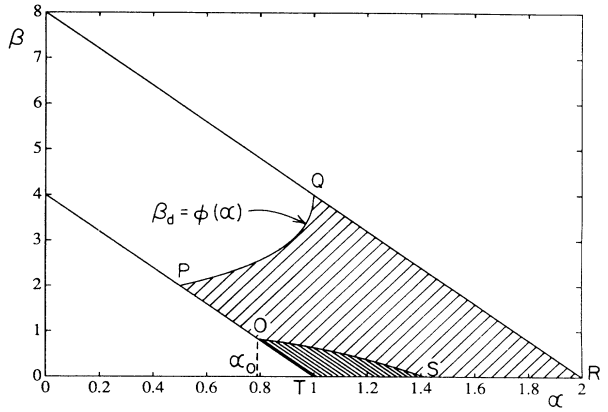

FIG. 5. Regions in the α-β parameter plane depicting various types of solutions of the map f. Region *PQRST* represents the region of chaotic behavior. Region *OST* represents a two-piece chaotic attractor in which each piece is visited every other iteration.

Figure 5 describes the various regions in the α-β parameter space and shows the types of solutions in each region.

We now computationally explore and confirm, for fixed values of α, the dynamics of the map f for the region in Fig. 5 where $\alpha\le\alpha_O$ (that is, the parameter space to the left of the point O in the figure). Figures 6–12 show the manner in which (a) the unstable solution x_1^* is created, (b) x_1^* influences the dynamics, (c) β influences the chaotic band, and the zones of attraction, (d) the inception of chaos occurs at $\beta=\beta_c$, and (e) the end of chaos is signaled beyond $\beta=\beta_d$. The method of cell mapping is used to provide periodic solutions of the map f as a function of the parameter β. The cell-mapping technique relies on the discretization of the state space to unravel the dynamics of nonlinear systems. An associated cell mapping of f can be readily generated to analyze the dynamics of f in terms of dynamics of cells which cover the space. A brief outline of the cell-mapping method used in the study is given in the Appendix. A more detailed account of the cell-mapping technique may be found in the research monograph by Hsu.[18]

Figure 6 shows the variation with β of the first five maps of f (starting with $x=x_A=\frac{1}{2}$) along with the locations of x_1^* and x_2^* for the case of $\alpha=0.2$. The result of applying the cell-mapping method to the map f is shown in Fig. 7. The state space of x is covered with 5000 intervals each of length 0.0002 and the space of parameter β into 1000 intervals each of length 0.072. In all, there are 5 million cells in the augmented-state space. What is displayed in the figure are locations of the center point of periodic cells discovered by the cell-mapping method. We observe the persisting stable trivial solution at $x=0$ along with other periodic solutions as detected by the cell mapping. The prominent ones are the unstable fixed points x_1^* and x_2^* represented by the two dark lines. The locations of various fixed points and periodic solutions provided by the cell-mapping method are approximate. However, these locations can be further refined by using an iterative technique like the Newton-Raphson method. These approximate locations of periodic solutions serve

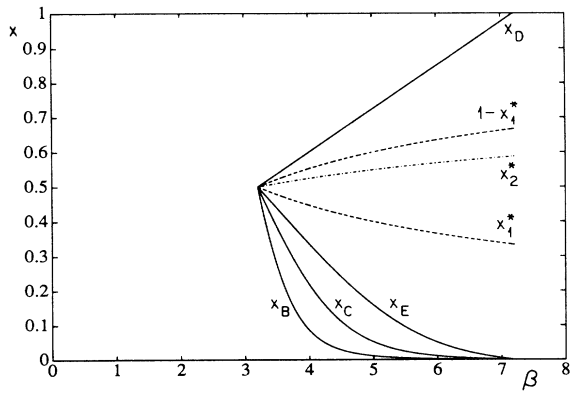

FIG. 6. Variation of the first five maps of f with β staring at $x=\frac{1}{2}$ for the case $\alpha=0.2$.

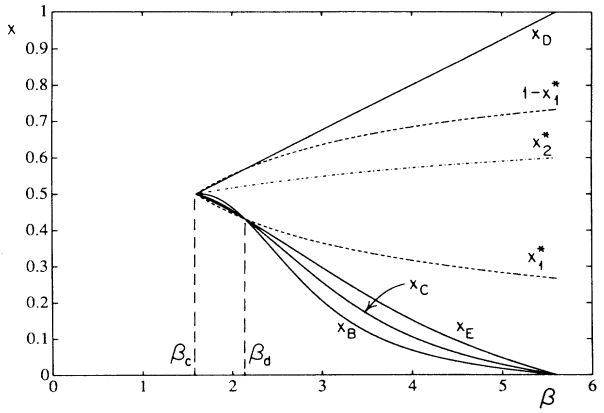

FIG. 8. Variation of the first five maps of f with β starting at $x=\frac{1}{2}$ for the case $\alpha=0.6$.

as very good initial guesses to any iterative technique employed for solving a system of nonlinear algebraic equations. The refined solutions may then be used for studying stability of periodic orbits. We have found that the various periodic solutions detected by the cell-mapping method are all unstable except the one at $x=0$ which is asymptotically stable. For the case of $\alpha=0.2$, the fixed point at $x=0$ is a stable global attractor, thus confirming our analytical results.

Figures 8–10 are for the case $\alpha=0.6$. According to Fig. 5, there exists a chaotic attractor for this value of α. The cell-mapping result given in Fig. 9 indicates the beginning of chaos at $\beta=\beta_c=1.6$ and the end of chaos at $\beta=\beta_d=2.146\,700\,167\,7$. The band of points in the region $\beta_c<\beta<\beta_d$ provided by the cell mapping consists of a collection of a large core of periodic cells and is seen as an attractor with a very high period. The center point of the location of each of the periodic cells is shown in this figure. Discretization of space due to its cellular structure splits a continuous band of attractor in $\mathbb{Q}$ (the set of real numbers) into several discrete set of periodic cells. The figure also shows a trapped region of trajectories bounded by the line x_D and x_E of Fig. 8. Whether or not

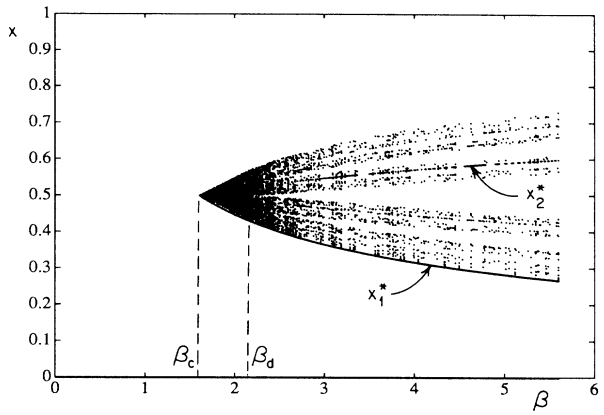

FIG. 9. Cell-mapping result showing periodic solutions of the map f as a function of β for the case $\alpha=0.6$.

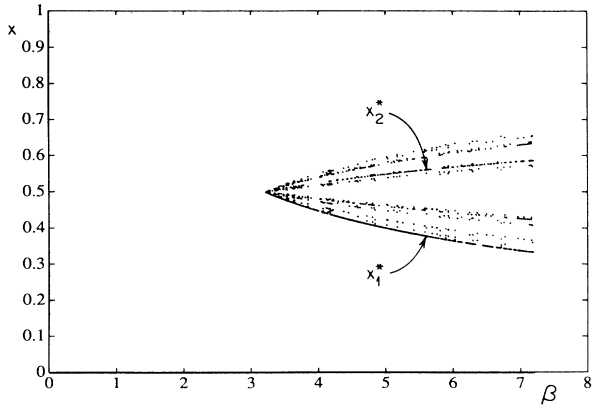

FIG. 7. Cell-mapping result showing periodic solutions of the map f as a function of β for the case $\alpha=0.2$.

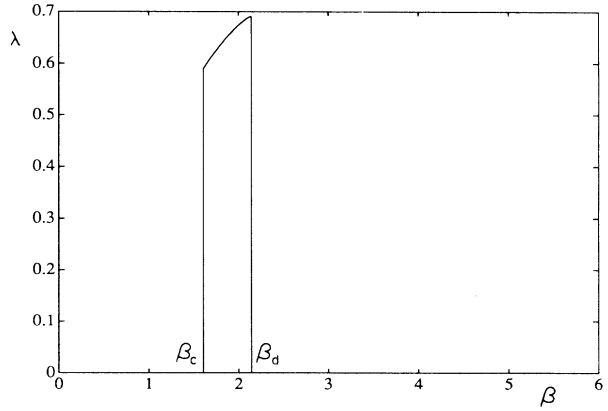

FIG. 10. Liapunov exponent λ as a function of β for the case $\alpha=0.6$.

the thick band of points contain a strange attractor is verified computationally by studying the sensitivity of trajectories to initial conditions. Figure 10 shows the Liapunov exponent λ as a function of the parameter β. As observed, the Liapunov exponent is positive in the region $\beta_c < \beta < \beta_d$ indicating that the attractor in this region is a strange attractor covering the region $[x_D, x_E]$. The cell-mapping result in Fig. 9 also confirms the region of attraction of the fixed point at $x = 0$ [the intervals attracted being $(0, x_1^*)$ and $(1-x_1^*, 1)$] and the chaotic attractor [the interval attracted being $(x_1^*, 1-x_1^*)$]. Thus, both a stable fixed point and a strange attractor coexists for a large range of values of the parameter β. The fixed point at $x = 0$ becomes a global attractor for $\beta > \beta_d$ when the chaotic attractor disappears.

Figures 11 and 12 are for the case $\alpha = 0.75$. Here again the cell-mapping result in Fig. 12 indicates the inception of chaos at $\beta = \beta_c = 1.0$ and the termination of chaos at $\beta = \beta_d = 2.438\,447\,187\,2$. The Liapunov exponent computation already provided in Fig. 4(b) supports the cell-mapping result indicating that the attractor is chaotic for values of β in the region $\beta_c < \beta < \beta_d$. The cell-mapping analysis also provides the regions of attraction associated with the fixed point at $x = 0$ and the chaotic attractor. The results agree with Fig. 5.

We now turn to an interesting feature of the map f, which can be explained in terms of the iterates of the point E, namely, C and B. As observed in Fig. 5, chaos begins for α values to the right of point P, when the β values lie in the shaded region $PQRTP$. Furthermore, for any value of α to the right of P, for $0 < \beta < \beta_c$ all trajectories are attracted to the stable fixed point at $x = 0$. The inception of chaos occurs when $\beta > \beta_c$. Yet, as β increases, the map of point E, namely, C, may lie to the left or the right of point B. Now segment AD maps to segment ED (by segment we mean the segment along the map), AE maps to CD and CD maps to BE. Thus, if $x_C < x_B$, we have $AE \to CD \to EB$ and the attractor has only one piece. If, however, $x_C > x_B > \frac{1}{2}$ then clearly

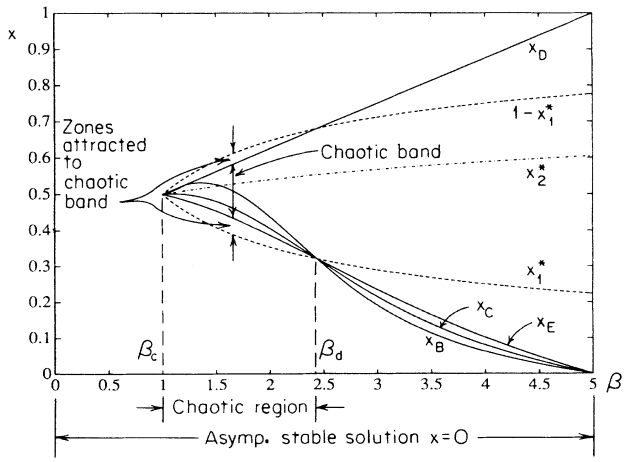

FIG. 11. Variation of the first five maps of f with β starting at $x = \frac{1}{2}$ for the case $\alpha = 0.75$.

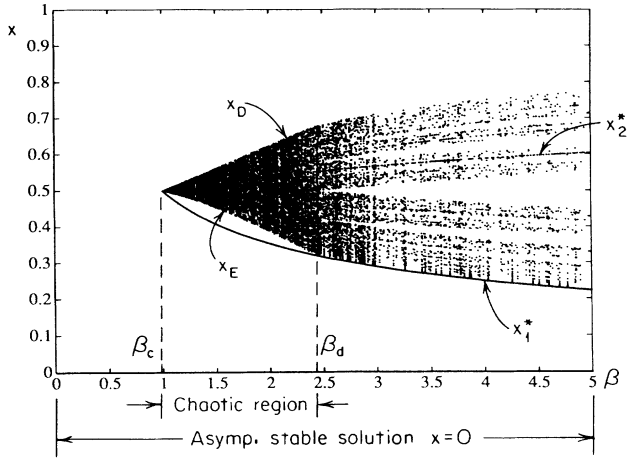

FIG. 12. Cell-mapping result showing periodic solutions of the map f as a function of β for the case $\alpha = 0.75$.

$x_B < x_2^* < x_C$ and hence the map of B, namely, F, has $x_F > x_C$ because $|f'(x)| > 1$ for $x \in (x_B, x_C)$. Thus the segment $CD \to BE \to FC$ and we have a two-piece attractor since segment BE is disjoint from segment CD leading to the following result.

Theorem 7. (a) If $x_B > x_C$ and α and β are in the chaotic region of Fig. 5, then the attractor is a one-piece attractor formed by the segment $[x_E, x_D]$. (b) If $x_C > x_B > \frac{1}{2}$ and α and β are in the chaotic region of Fig. 5, then the attractor is a two-piece attractor formed by the segments $[x_E, x_B]$ and $[x_C, x_D]$.

Proof. (a) The first assertion has already been proved above. The one-piece attractor is a period one attractor. (b) Note that $x_B < x_2^* < x_C$ and that x_2^* is unstable. Thus almost all trajectories that begin in the interval (x_B, x_C) will leave the region, so that asymptotically all trajectories will be attracted to the two-piece attractor from our previous discussion. The two-piece attractor is a period two attractor whose trajectory visits each of its two pieces alternately. ■

The limiting condition for a two-piece attractor would be $x_B = x_C = x_2^*$. This condition yields a polynomial in α and β which is of order 40 when α is fixed and of order 27 when β is fixed. The polynomial is computed by using the symbolic computer language MACSYMA. The appropriate positive real root of this polynomial is plotted in Fig. 5 by line OS. At point O, $x_2^* = x_B = x_C = x_A$, the value of α is obtained by setting

$$\left[\frac{\partial x_2^*}{\partial \beta}\right]_{\beta=\beta_c} = \left[\frac{\partial y_E}{\partial \beta}\right]_{\beta=\beta_c}. \tag{13}$$

The left-hand side can be obtained by differentiating the relation (6) and the expression on the right-hand side is calculated by using MACSYMA. This yields

$$\frac{1}{16(2-\alpha)} = \tfrac{1}{8}(-4\alpha^2 + 10\alpha - 5) \tag{14}$$

whose only root within the domain of interest is $\alpha = (3-\sqrt{2})/2 = 0.792\,893\,218\,8$. The point S in Fig. 5 is obtained by considering

$$(x_B)_{\beta=0}=(x_C)_{\beta=0} \tag{15}$$

which results in the polynomial $\alpha(\alpha^3-\alpha^2-2\alpha+2)=0$. This has only one real root of interest given by $\alpha=\sqrt{2}$.

Furthermore, it is possible to show using MACSYMA that along the line OS where $x_B=x_C$ (see Fig. 5), $\partial x_B/\partial\beta > \partial x_C/\partial\beta$ so that for the region outside OST, $x_B > x_C$ and the map f has a one-piece chaotic attractor (see Figs. 8 and 11). A plot of the variation of these slopes, evaluated along OS as a function of α is shown in Fig. 13. On the other hand, $x_C > x_B > \frac{1}{2}$ for points that lie in the region OST and the map f has a two-piece chaotic attractor. From computational results provided below, we confirm our understanding of the dynamics of the map f in these cases.

We first consider the case $\alpha=0.9$. Figure 14 shows the variation in x_B, x_C, x_D, x_E, x_1^*, and x_2^* as a function of β. The cell-mapping result is given in Figs. 15(a) and 15(b). It is difficult to observe that Fig. 15(a) includes a peculiar island structure near $\beta=\beta_c$. In order to see this region clearly, a separate cell-mapping analysis is carried out over this region with a finer cellular structure and the result is indicated in Fig. 15(b) showing the existence of a two-piece attractor. For values of β that fall above the line OS, the island of repulsion disappears confirming our results of Theorem 7. The unstable solution x_2^*, separating the two pieces of the attractor, is also provided by the cell-mapping method. Chaos begins at $\beta=\beta_c=0.4$ and stops at $\beta=\beta_d=2.919\,275\,152\,5$, and cell-mapping results indicate this by providing many periodic cells in this range. Liapunov exponent for this region is positive as shown in Fig. 16. The two-piece chaotic attractor exists in the range $\beta_c<\beta<\beta_h$ (Fig. 14), where $\beta_h=0.742\,045\,770\,2$ and coalesces into a one-piece chaotic attractor for $\beta>\beta_h$. For $\beta=0.6$, Fig. 17(a) shows the portion of the map containing the chaotic band which in this case is a two-piece chaotic attractor. The long-term probability distribution of this attractor is shown in Fig. 17(b). For $\beta=1.0$, Figs. 17(c) and 17(d) show, respectively, the one-piece chaotic attractor and its long-term probability distribution.

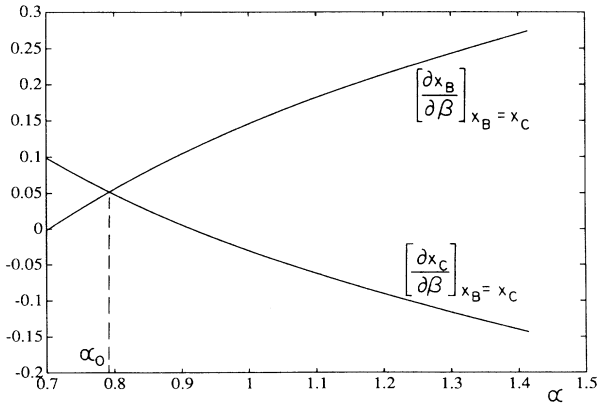

FIG. 13. Rate change of x_B and x_C with respect to β as a function of α evaluated for $\beta=\beta_c$.

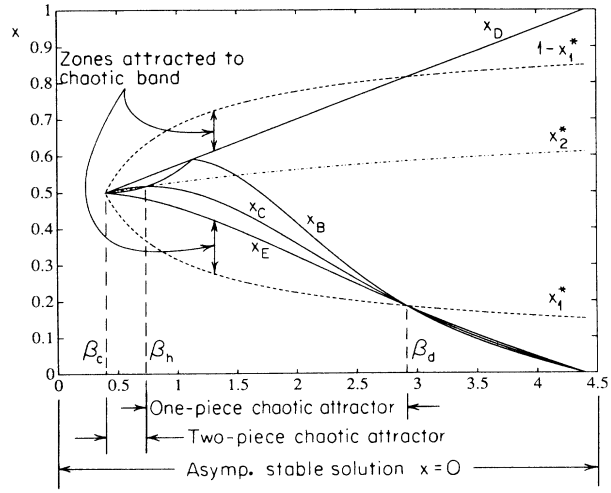

FIG. 14. Variation of the first five maps of f with β starting at $x=\frac{1}{2}$ for the case $\alpha=0.90$.

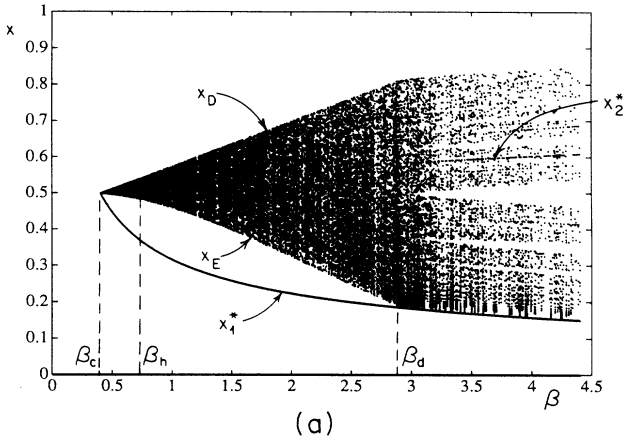

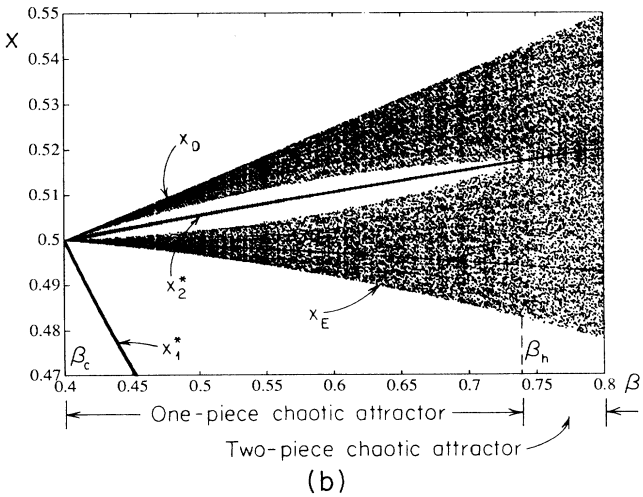

FIG. 15. (a) Cell-mapping result showing periodic solutions of the map f as a function of β for the case $\alpha=0.90$. (b) Cell-mapping result showing the two-piece attractor of the map f as a function of β for the case $\alpha=0.90$.

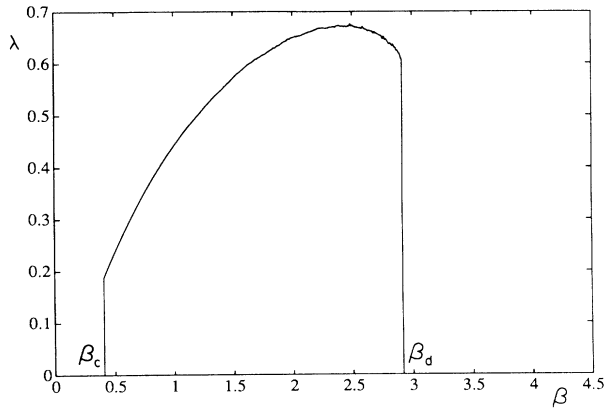

FIG. 16. Liapunuv exponent λ as a function of β for the case $\alpha=0.90$.

For $\alpha=1.1$, Figs. 18–20 show the variations as in Fig. 14, the cell-mapping results, and the Liapunov exponent as a function of β. The trivial solution at $x=0$ is unstable and as expected, chaotic behavior is observed for all $\beta\in[0,4(2-\alpha)]$. The sensitive dependence of the trajectories of (1) results in the positive Liapunov exponent throughout this region. The strange attractor is a two-piece one beginning at $\beta=0$ and becomes a single-piece attractor for $\beta>\beta_h$, where $\beta_h=0.520\,359\,588\,2$.

For $\alpha=1.5$, Figs. 21–23 depict the computational results in the same order as in Figs. 18–20. As observed from the cell-mapping results shown in Fig. 22, the island structure found for the case $\alpha=1.1$ disappears here. The only attractor that exists for all $\beta\in[0,4(2-\alpha)]$ is a one-piece chaotic attractor. These results confirm Theorem 7.

As a final check, we performed an exhaustive search to verify computationally the region *PQRSTO* in Fig. 5 where a chaotic attractor exists. First, the entire α-β parameter plane covering the region $0<\alpha<2$ and $0<\beta<8$ is divided into a grid consisting of 1000×1000 points. For each value of the parameter set (α,β), we checked if one of the conditions $x_C>x_B>\frac{1}{2}$ or $x_B>x_C$ is satisfied. The region in the α-β plane where the condition $x_C>x_B>\frac{1}{2}$ is met coincides with the region *OST* of Fig. 5 where a two-piece chaotic attractor is expected. The points in the α-β plane where the condition $x_B>x_C$ is satisfied again coincides with the region *PQRSO* of Fig. 5 indicating the presence of one-piece chaotic attractor. In

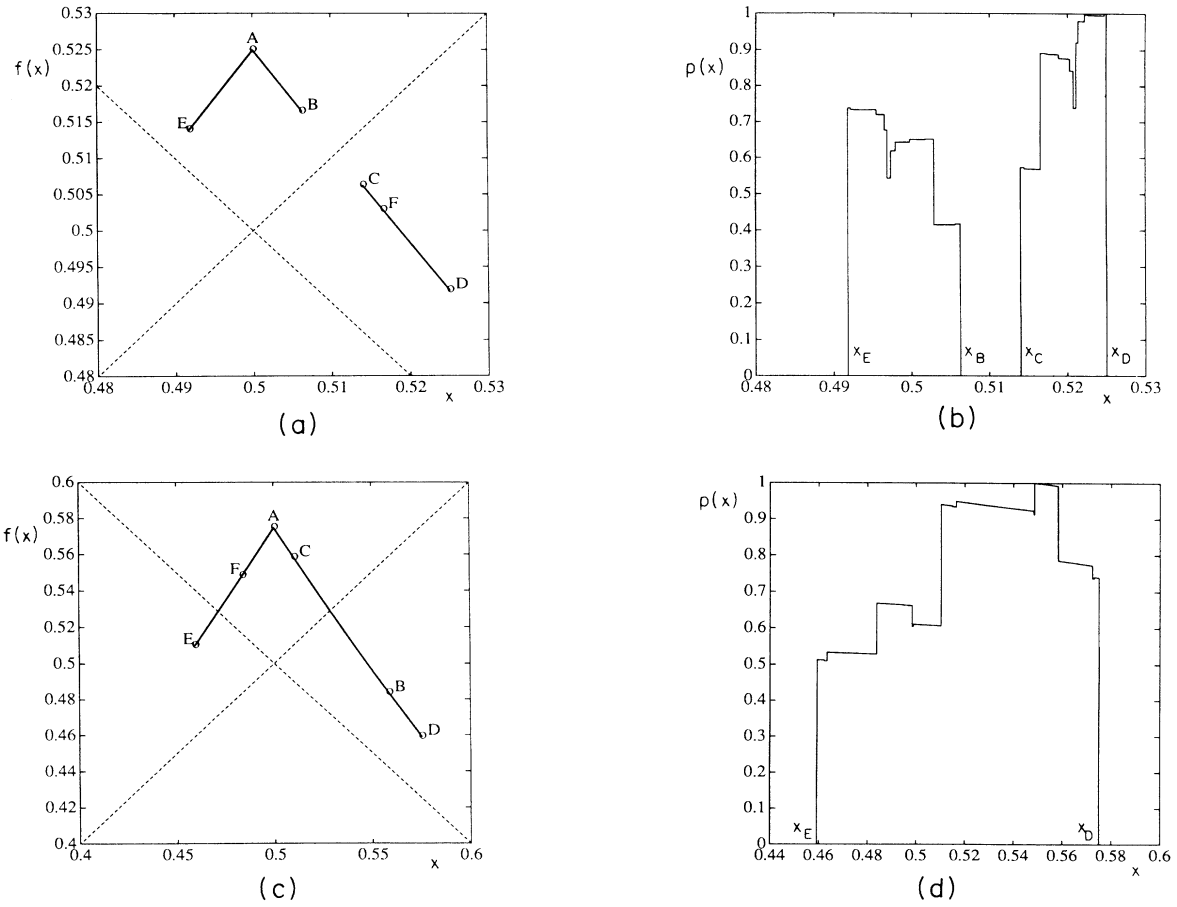

FIG. 17. (a) Two-piece chaotic attractor for $\alpha=0.90$ and $\beta=0.6$. (b) Long-term probability distribution of the two-piece chaotic attractor for $\alpha=0.90$ and $\beta=0.6$. (c) One-piece chaotic attractor for $\alpha=0.90$ and $\beta=1.0$. (d) Long-term probability distribution of the one-piece chaotic attractor for $\alpha=0.90$ and $\beta=0.6$.

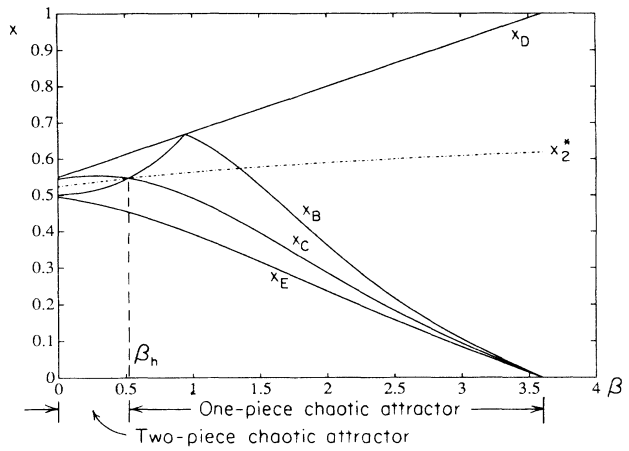

FIG. 18. Variation of the first five maps of f with β starting at $x=\frac{1}{2}$ for the case $\alpha=1.1$.

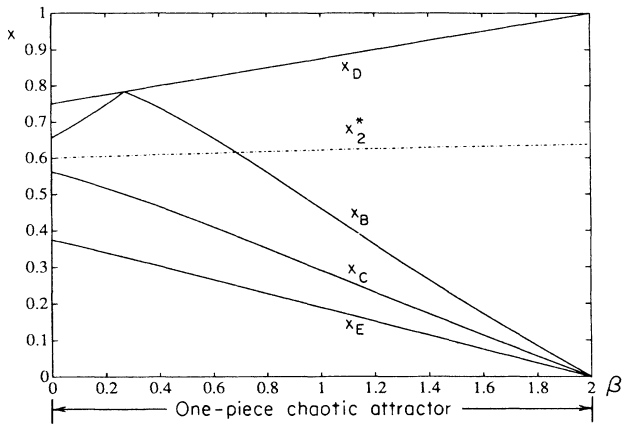

FIG. 21. Variation of the first five maps of f with β starting at $x=\frac{1}{2}$ for the case $\alpha=1.5$.

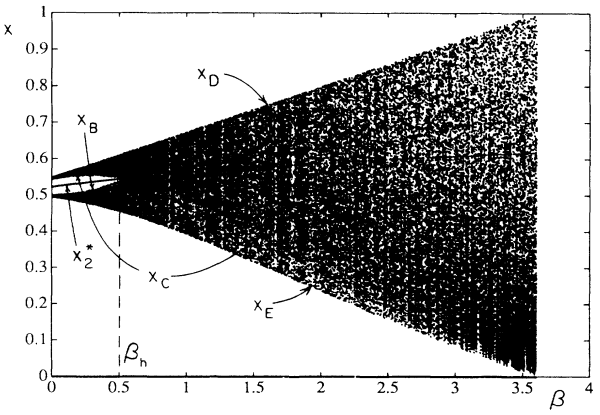

FIG. 19. Cell-mapping result showing periodic solutions of the map f as a function of β for the case $\alpha=1.1$.

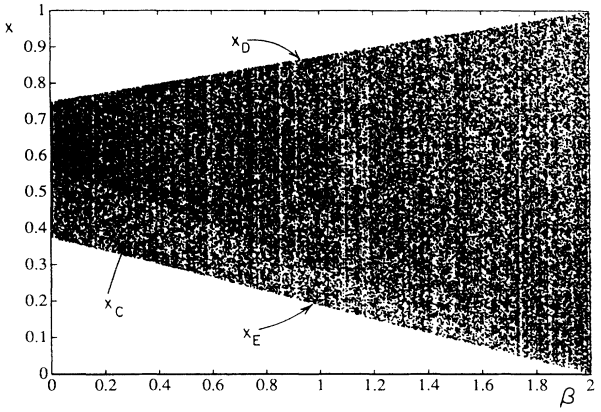

FIG. 22. Cell-mapping results showing periodic solutions of the map f as a function of β for the case $\alpha=1.5$.

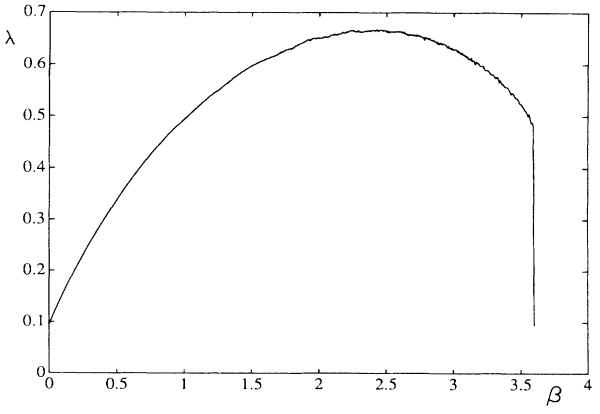

FIG. 20. Liapunov exponent λ as a function of β for the case $\alpha=1.1$.

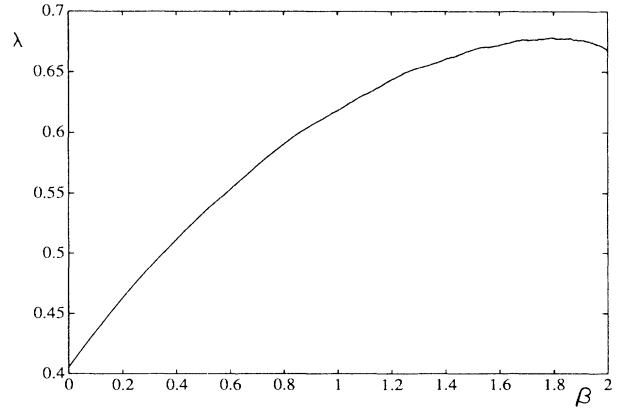

FIG. 23. Liapunov exponent λ as a function of β for the case $\alpha=1.5$.

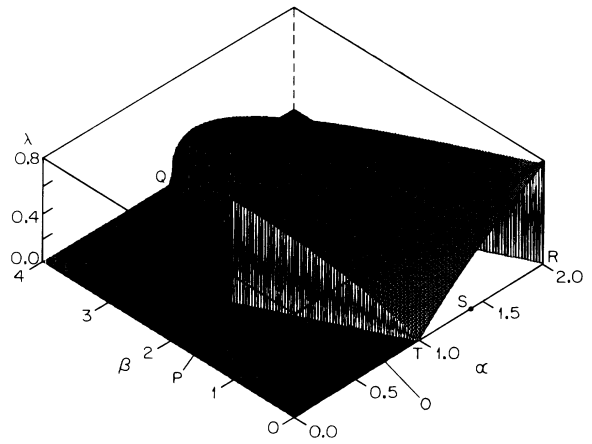

FIG. 24. Three-dimensional plot of Liapunov exponent λ as a function of α and β corresponding to the region *PQRSTO* of Fig. 6.

both cases, the fixed point at $x=0$ is also an attractor for values of $\alpha<1$. Further, for each point in the region *PQRSTO*, the computed Liapunov exponent was found to be positive, confirming our results of Theorem 7. A three-dimensional plot of the Liapunov exponent as a function of α and β is shown in Fig. 24.

It is indeed both strange and aesthetic that the two simple conditions mentioned in Theorem 7 thus provide surprising yet strong evidence for the existence of a chaotic attractor for the piecewise cubic map. It is comforting to know that by observing only the first few maps of the function f, one can predict the overall global behavior of its dynamics. The analytical studies presented in this paper have thus been well substantiated by numerical computations despite the fact that the dynamics of the map depends on two independent parameters.

III. CONCLUDING REMARKS

A detailed analysis of the dynamics of a cubic map represented by two parameters is carried out in this paper, both analytically and numerically, to understand the route it follows to chaos. Such maps are important in several fields, especially in the study of nonlinear mechanical systems. The study indicates that the route to chaos followed here is not representable by the standardly proposed routes, namely, type I, type II, or type III intermittency.[19–23] The chaos in the cubic map is initiated by the appearance of an unstable solution which is suddenly born out of a tangent bifurcation. This unstable fixed point demarcates the zones of attraction of the chaotic attractor and the asymptotically stable trivial fixed point at zero. The disappearance of chaos is signaled by the condition $x_D=x_E$.

The general approach presented in this paper does not depend on the nature of the map itself, that is, whether its Schwarzian derivative is negative or not, see Singer.[24] Though we have illustrated it for the cubic map here, the methodology could be used to good advantage in unraveling the dynamics of other types of maps as well. What is extraordinary here is that one can deduce the global behavior of the cubic map by simply analyzing the first few maps. Elucidation of dynamics of the map is greatly simplified through a multiprong attack by analytical, symbolic, and computational tools. This combination of analytical and numerical tools seems to be very useful in describing the characteristics of nonlinear systems in the physical sciences.

ACKNOWLEDGMENTS

This research was supported by the National Science Foundation and the USC Faculty Research and Innovation Fund.

APPENDIX: CELL-MAPPING TECHNIQUE

1. Introduction

The purpose of utilizing the cell-mapping method for studying the cubic map given by Eq. (1) is to obtain information about its global behavior, especially as a function of the two parameters α and β. The cell mapping also enables us to get an idea about some of the unstable solutions which happen to be very important for the cubic map studied in this paper. For example, referring to Fig. 12 obtained by the cell-mapping method both the unstable solutions x_1^* and x_2^*, which essentially control the global dynamics of the map, are visible. The existence of the unstable solution x_1^* signals the birth of the chaotic behavior of the map. As shown in Fig. 15(b), the role of the unstable solution x_2^* in depicting the existence of the two-piece chaotic attractor is made clear. In addition, the cell-mapping method indicates that there are a few characteristic lines (or curves) in the β-x plane which are essentially the first few iterates of the peak of the map. These first few iterates are sufficient to describe the overall global behavior of the map. It is quite obvious, again referring to Fig. 12, that the cell-mapping method provides the regions of attraction of the stable fixed point at $x=0$ and the chaotic attractor. Also, it gives insight into how the chaotic band grows and how its collision with the unstable solution x_1^* causes its disappearance. Straightforward iteration would not only miss the unstable solutions but also require an inordinate amount of computations to arrive at the above conclusions.

In this appendix we discuss the general computational technique based on discretization of the state space which was extensively employed in Sec. II to confirm several of our analytical results for the global analysis of the piecewise cubic map. The method of cell mapping is also applicable to nonlinear dynamical systems described by differential equations. Multidimensional maps of the form

$$\mathbf{x}(n+1)=\mathbf{G}(\mathbf{x}(n)), \quad n=0,1,2\ldots \tag{16}$$

where $\mathbf{x}\in\mathbb{Q}^N$ and $\mathbf{G}:\mathbb{Q}^N\rightarrow\mathbb{Q}^N$ will be considered here for further discussion.

2. Brief review of cell mapping

A powerful computational approach for analyzing the global behavior of dynamical systems is provided by the cell-mapping technique.[25] In this formulation, the state space is thought of not as a continuum but instead as a collection of *cells*. Each cell occupies a prescribed region of state space as defined by Eq. (17). Every cell in the discretized state space or *cell state space* is to be treated as a state entity. The motivation for discretizing the state space in terms of cells is supported by the facts that in practice state variables can be measured only to a certain accuracy and that round off errors arise in the computation of the state variables using digital computers. These two facts force one to abandon the idea of state space as being a continuum as far as studying global properties of dynamical systems from a computational point of view.

In order to construct a cellularly structured state space S, let the coordinate axes of the state variable components x_i, $i=1,\ldots,N$ be divided into a large number of intervals of uniform size h_i. The new state variable z_i along the x_i axis is defined to contain all x_i such that

$$(z_i-\tfrac{1}{2})h_i \le x_i < (z_i+\tfrac{1}{2})h_i \ . \tag{17}$$

By definition, z_i in (17) is an integer. A cell vector z is defined to be an N tuple z_i, $i=1,\ldots,N$. Clearly, a point $\mathbf{x}\in\mathbb{Q}^N$ with components x_i belongs to a cell $z\in S$ with components z_i if and only if x_i and z_i satisfy (17) for all i. The space S consisting of elements which are N tuple of integers is referred to as an N-dimensional cell space. If N_{c_i} denotes the number of intervals along the x_i axis, then the cell space S contains a total of $N_{c_1}\times N_{c_2}\times\cdots\times N_{c_N}$ cells.

In the cell state space S, one can define a cell-to-cell mapping dynamical system in the form

$$z(n+1)=C(z(n)),\quad C:S\to S,\quad n\in\mathbb{Z} \tag{18}$$

where C is referred to as a *simple cell mapping*. It can also be perceived of as a mapping from a set of integers to a set of integers. Equation (18) then describes the evolution of a cell dynamical system in N-dimensional cell state space S. For a detailed treatment concerning the properties of the map C and its refinements, the reader is referred to the research monograph by Hsu.[18] In the following sections, we concentrate on the simple cell-mapping method only and refer to it simply as cell mapping.

3. Periodic motion

Dynamics of the cell-mapping system (18) is characterized by singular cells consisting of equilibrium cells and periodic cells. An *equilibrium cell* z^* is given by $z^*=C(z^*)$. A *periodic cell* of period $K\in\mathbb{Z}^+$ (or simply a P-K cell) is a set of K distinct cells $\{z^*(k)|k=1,2,\ldots,K\}$ such that

$$\begin{aligned} &z^*(k+1)=C^k(z^*(1)),\quad k=1,2,\ldots,K-1\\ &z^*(1)=C^K(z^*(1))\ , \end{aligned} \tag{19}$$

where C^k means the mapping C applied k times. This set is said to constitute a *periodic motion* of period K or simply a P-K motion. An equilibrium cell in this context is a P-1 cell. A *regular cell* is one which is not singular.

Two cells z and z' are said to be *contiguous* if and only if $z-z'=\pm\mathbf{e}_j$, for some $j=1,2,\ldots,N$, where $\mathbf{e}_j$ is a unit vector coinciding with the x_j axis. Then, an equilibrium cell is an *isolated* or a *solitary* cell if none of its contiguous cells are equilibrium cells. An equilibrium cell, when not isolated, may have several contiguous equilibrium cells. Then, a complete set of contiguous equilibrium cells is referred to as a *core of equilibrium cells*. The size of the core is determined by the number of cells in it. Similar definitions apply to periodic cells.

4. Creating a cell mapping for a map

To obtain a cell mapping associated with the map (16) the following procedure may be employed. First, construct a cell space structure in the state space region with cell size h_i in the x_i direction. Let $\mathbf{x}^d(n)$ denote the center point of the cell $z(n)$ so that $x_i^d(n)=h_i z_i(n)$. Suppose that the trajectory starting from $\mathbf{x}^d(n)$ terminates at $\mathbf{x}^d(n+1)$ when the mapping $\mathbf{G}$ is applied once. The cell in which $\mathbf{x}^d(n+1)$ lies is taken to be $z(n+1)$, the image cell of $z(n)$. Specifically

$$z_i(n+1)=C_i(z(n))=\text{int}\left[\frac{x_i^d(n+1)}{h_i}+\frac{1}{2}\right], \tag{20}$$

where $\text{int}(u)$, for any real number u, represents the largest integer such that $\text{int}(u)\le u$. This process of finding image cells is repeated for every cell in the cell state space S. The mapping C so obtained is a cell mapping associated with the dynamical system (16) using the *center point method* described above to compute the image cells.

5. Analysis of the cell mapping

A trajectory of the cell-to-cell mapping dynamical system (18) starting from an initial cell state $z(0)$ is referred to as a *cell sequence* of (18) and it is the set of integers given by $\{z(k)\}$, $k=0,1,2,\ldots$. Once the mapping C in (18) is obtained, the crucial step in cell-mapping analysis is to unravel the dynamic information of the original system (16) contained in (18) by examining the long-time behavior of the cell sequences. Every cell in the cell state space S is to be classified as a regular cell (meaning it is a transient cell) or a singular cell.

In practical applications, the state variables assumes a finite range of values. Hence, one is usually interested in a fixed state space region which contains a finite number of cells even though the number of cells may be huge. The complement of the fixed state space is referred to as the *sink cell*. Once a cell in S maps to the sink cell, its long-time behavior is unknown and its motion is eventually locked in the sink cell. An important property of the cell sequences, due to the finite number of cells in the state space, is that all cell sequences must terminate with a finite number of cell mappings into one of the steady cell states: equilibrium cell, periodic cells, or the sink cell. This is the key to the global cell-mapping algorithm described by Hsu and Guttalu[26] from which the following

characteristics of the dynamics of the system (16) can be obtained all at once: (1) location of the equilibrium states and periodic solutions in a given state space, (2) domains of attraction associated with the asymptotically stable equilibriums states and periodic solutions, and (3) step-by-step evolution of the global behavior of the system starting from any initial state within the cell state space.

To further elaborate on the step-by-step evolution of the system, let *r-step domain of attraction* be defined as the set of all cells in S which map to a P-K motion in r steps or less. Then, the *total domain of attraction* of a P-K motion is its r-step domain of attraction in the limit as $r \rightarrow \infty$. The periodic cells are represented by the 0-step domain of attraction. As r increases, one obtains the evolution of the domains of attraction which contain an increasing number of cells. Since the cell state space S consists of a finite number of cells, it should be noted that the total domain of attraction of a P-K motion is given by the largest of the r-step domains of attraction (with a finite value of r).

The associated cell mapping C given by (18) is viewed as an approximation of the original dynamical system (16). The degree of approximation can be improved by simply reducing the cell size h_i (equivalently, increasing the number of cells in S). The cell mapping C as defined by (18), in general, replaces the stable equilibrium points and stable periodic solution of (16) in the state space $\mathbb{Q}^N$ with sets of periodic cells in the cell state space S; unstable equilibrium points and unstable periodic solutions of (16) may not be recovered. Each set of periodic cells may consist of a group or core of "true periodic cells" representing the original periodic motion of the dynamical system (16) and core of "pseudo-periodic-cells" which surround the true periodic cells. These pseudo-periodic cells are the result of discretization of the state space; the state space occupied by them has been shown to shrink as the cell size is made smaller.[25]

The method of cell mapping applies to strongly nonlinear dynamical systems, and to both autonomous and nonautonomous systems. Since this method avoids repetitive time-consuming calculation of the trajectories of dynamical systems, it has been found to be an efficient computational tool. The global cell-mapping algorithm is applicable to a compact region of the state space.

For the cubic map which maps the unit interval to the unit interval, it is important to note that there is no need to introduce the concept of the sink cell since the state space is compact.

6. Parameter study

The cell-mapping method provides a convenient way to analyze maps which depend on parameters. Each parameter may be considered as a distinct state variable along which the map is an identity map. A new element x_{N+1} may be added to the state space such that

$$x_{N+1}(n+1)=x_{N+1}(n) \ . \tag{21}$$

The state space dimension is now increased by one. More parameters can be added in the same way. This is a convenient way to introduce parameters into the state equations from a computational point of view when the cell-mapping method is employed. The parameters are now discretized in the same way as the state variables. Since no additional computations are required by introducing equations of the form (21), the cell-mapping method will be an efficient computational scheme for global analysis of the map. The method discussed above may now be employed to obtain the periodic solutions of the map (16) as a function of the system parameters.

[1]J. Bernussou, *Point Mapping Stability* (Pergamon, Oxford, 1975).

[2]P. Collet and J. P. Eckmann, *Iterated Maps on the Interval as Dynamical Systems* (Birkhauser, Basel, 1980).

[3]R. L. Devaney, *An Introduction to Chaotic Dynamical Systems* (Benjamin-Cummings, Menlo Park, CA, 1986).

[4]P. Berge, Y. Pomeau, and C. Vidal, *Order within Chaos* (Wiley, New York, 1987).

[5]J. Guckenheimer and P. Holmes, *Nonlinear Oscillations, Dynamical Systems, and Bifurcation of Vector Fields* (Springer-Verlag, New York, 1983).

[6]A. J. Lichtenberg and M. A. Lieberman, *Regular and Stochastic Motion* (Springer-Verlag, New York, 1983).

[7]F. C. Moon, *Chaotic Vibrations* (Wiley, New York, 1987).

[8]J. M. T. Thompson and H. B. Stewart, *Nonlinear Dynamics and Chaos* (Wiley, Chichester, England, 1986).

[9]G. M. Zaslavsky, *Chaos in Dynamic Systems* (Harwood Academic, Chur, Switzerland, 1985).

[10]O. Chavoya-Aceves and F. Angulus-Brown, Physica D **14**, 374 (1985).

[11]F. T. Arecchi, R. Badii, and A. Politi, Phys. Rev. A **29**, 1006 (1984).

[12]J. Testa and G. A. Held, Phys. Rev. A **28**, 3085 (1983).

[13]B. Hu and J. M. Mao, Phys. Rev. A **27**, 1700 (1983).

[14]A. S. Pikovsky, J. Phys. A **16**, L109 (1983).

[15]S. Fraser and R. Kapral, Phys. Rev. A **25**, 3223 (1982).

[16]T. D. Rogers and D. C. Whitley, Math. Modeling **4**, 9 (1983).

[17]P. Holmes, Philos. Trans. R. Soc. London **292**, 419 (1979).

[18]C. S. Hsu, *Cell-to-Cell Mapping: A Method of Global Analysis of Nonlinear Systems* (Springer-Verlag, New York, 1987).

[19]J. H. Curry and J. A. Yorke, in *The Structure of Attractors in Dynamical Systems,* Vol. 668 of *Springer Notes in Mathematics,* edited by A. Dold and B. Eckmann (Springer-Verlag, Berlin, 1977), pp. 48-66.

[20]L. D. Landau and E. M. Lifshitz, *Fluid Mechanics* (MIR, Moscow, 1971).

[21]T. Li and J. A. Yorke, Am. Math. Monthly **82**, 985 (1975).

[22]S. E. Newhouse, D. Ruelle, and F. Takens, Commun. Math. Phys. **64**, 35 (1978).

[23]D. Ruelle and F. Takens, Commun. Math. Phys. **20**, 167 (1971); **23**, 343 (1971).

[24]D. Singer, SIAM (Soc. Ind. Appl. Math.) J. Appl. Math. **35**, 260 (1978).

[25]C. S. Hsu, J. Appl. Mech. **47**, 931 (1980).

[26]C. S. Hsu and R. S. Guttalu, J. Appl. Mech. **47**, 940 (1980).